Deep–Sea Research I 175 (2021) 103573

Contents lists available at ScienceDirect

Deep-Sea Research Part I

journal homepage: www.elsevier.com/locate/dsri

Trends in the Agulhas Return Current

Yotam Fadida [a,b,*,1], Neil Malan [a,c,d,e,2], Meghan F. Cronin [f,3], Juliet Hermes [a,c,3]

[a] University of Cape Town, South Africa
[b] Israel Oceanographic and Limnological Research, Israel
[c] South African Environmental Observation Network, South Africa
[d] Nansen-Tutu Centre for Marine Environmental Research, University of Cape Town, South Africa
[e] Coastal and Regional Oceanography Laboratory, School of Mathematics and Statistics, UNSW Sydney, Australia
[f] NOAA Pacific Marine Environmental Laboratory, Seattle WA, USA

ARTICLE INFO

Keywords:
Agulhas Return Current
Eddy kinetic energy
Western boundary extension

ABSTRACT

Recent observations report a poleward shift in several of the world's western boundary current extensions in response to a warming climate. However, the nature and variability of the Agulhas Return Current (ARC) is still relatively unknown, leading to uncertainty in its response to gyre intensification. The objective of this work is to investigate meridional migration and eddy kinetic energy (EKE) trends in the ARC over the past 27 years using satellite-derived altimetry products. A difference is seen between the western and eastern regions of the ARC, the former exhibiting a predominantly equatorward migration and the latter moving predominantly poleward. The ARC is shown to be a region highly influenced by its bathymetry. Additionally, we show that the regional EKE peaks during austral summer months and that there has been a significant rise in summertime EKE levels between 1994–2011.

1. Introduction

Western boundary currents (WBC) and their extensions are found in each of the five ocean basins and transport warm water of tropical origin into the subtropical interior of the basin. WBC systems have amongst the highest values for mean velocity, eddy kinetic energy (EKE), air–sea heat flux, carbon uptake and nutrient transport (Dong and Kelly, 2003; Friehe et al., 1991; Wu et al., 2012; Takahashi et al., 2009). Due to the presence of strong sea surface temperature (SST) gradients across the current, these areas are characterized by intense air–sea interactions (Small et al., 2008) that can have significant impacts on regional weather, fishing industries and shipping routes (Chang et al., 2013; Oey et al., 2018). In addition, WBCs play a major role in the global carbon cycle (Dinezio et al., 2009) acting as a CO_2 sink (Takahashi et al., 2009) due to the slow loss of heat to the atmosphere and the relatively high levels of biological production in the euphotic zone (Gray and Palter, 2017).

The Agulhas Current (AC) western boundary system is unique, in that it retroflects, with a small portion of the current feeding into the South Atlantic in the form of Agulhas Rings and filaments (estimates ranging from 10–40 Sv, (Gordon, 1986; Speich et al., 2001; van Sebille et al., 2010; Richardson, 2007)) and the majority of the current turning east to become the Agulhas Return Current (ARC). In this way, the AC re-joins the South Indian subtropical gyre (Lutjeharms and Ansorge, 2001). Past studies of the long term changes to the global ocean circulation (Wu et al., 2012; Yang et al., 2016; Kwon and Deser, 2007; Yang et al., 2020) have shown that most WBCs are intensifying and migrating poleward. The main mechanism driving this change is thought to be an intensification and poleward shift of near-surface ocean winds, attributed to positive annular mode-like trends (Yang et al., 2016). This WBC intensification has been shown to manifest in different manners in each of the basins and is not robust to all WBC systems. Beal and Elipot (2016) have shown that over time, the Agulhas Current is not intensifying, but rather broadening, with an increase in mesoscale activity. Conflict exists between modeled and observed trends, in particular in the ARC, where only the section to the east of 40°E has been considered by past studies, rather than the whole length of the ARC (Yang et al., 2020), which is generally considered to begin between 15°E and 30°E (Boebel et al., 2003; Zhu et al., 2018).

In other WBC systems, based on hydrographic and satellite altimetry data, it has been shown that the southward penetration of the

* Corresponding author at: Israel Oceanographic and Limnological Research, Israel.
E-mail addresses: yotamfadida@ocean.org.il (Y. Fadida), neilcmalan@gmail.com (N. Malan), Meghan.F.Cronin@noaa.gov (M.F. Cronin), juliet@saeon.ac.za (J. Hermes).
[1] MSc.
[2] Postdoctoral Research Fellow, now at Coastal and Regional Oceanography Lab, School of Mathematics and Statistics, UNSW, Sydney, NSW, 2052 Australia.
[3] Ph.D.

https://doi.org/10.1016/j.dsr.2021.103573
Received 12 September 2020; Received in revised form 15 May 2021; Accepted 31 May 2021
Available online 17 June 2021
0967-0637/

East Australia Current (EAC) has increased over the last half century (Ridgway, 2007; Ridgway et al., 2008). The strength and poleward transport of its extension has also increased since the 1980s (Cetina-Heredia et al., 2014), with a sharp increase in eddy driven transport noted from 2005 onward. The Kuroshio Current and Kuroshio Current Extension's response to global warming was investigated (Sakamoto et al., 2005) with a high-resolution atmosphere–ocean coupled climate model and revealed an increase in current velocity of 0.3 m s^{-1} at 150°E. Additionally an intensification of the Kuroshio Extension during the 1980s relative to the 1970s was reported by Deser et al. (1999). The transport increase in the Kuroshio Current Extension was the result of an adjustment of the oceanic circulation to a decadal variation in the wind stress curl over the mid-latitude Pacific with a 4–5 year lag. As revealed through the use of a high resolution ocean–atmosphere coupled model, the Brazil-Malvinas confluence has migrated southward at a rate of approximately 0.6° per decade between 1992–2007 (Combes and Matano, 2014; Goni et al., 2011). A high resolution numerical experiment demonstrates that this migration is a result of a weakening in the Antarctic Circumpolar Current (ACC) across the Drake passage, driven by a weakening of the westerly winds over the Southeastern and Southwestern Pacific and the Atlantic Basins from 2000 onwards (Combes and Matano, 2014).

In contrast, over the central Pacific and Indian Ocean Basins, westerlies appear to be strengthening (Combes and Matano, 2014). Satellite altimetry data has also been used to reveal a poleward trend in the mean latitude of ACC transport (Gille, 2014). As a result of the increased wind stress curl over the Indian subtropics, the Agulhas Current has broadened rather than increased in transport or strength (Beal and Elipot, 2016). In particular, they show that the broadening is associated with an increased eddy energy, which appears to be due to the intensifying winds. Satellite altimetry observations from 1993–2009 reveal an intensification in mesoscale variability of the Agulhas system, particularly in the Mozambique channel and south of Madagascar, leading to accelerated eddy propagation. This intensification has been attributed to an increased South Equatorial Current driven by enhanced trade winds over the tropical Indian Ocean (Backeberg et al., 2012). In the Agulhas Retroflection region an increase in the Agulhas Leakage has been shown to occur due to an intensification of the Southern Hemisphere Westerlies (Biastoch et al., 2009). While many studies of the ARC region have put an emphasis on the air–sea interactions associated with the oceanic temperature front (Liu et al., 2007; Tozuka and Cronin, 2014; Ohishi et al., 2016), there is a gap when it comes to research into a meridional migration of the ARC.

This study focuses on the path of the ARC between the years 1993 and 2019. In particular, using 27-years of daily SSH fields, we evaluate the long-term mean ARC path and its variability and trends. In addition, we analyze the impact of the ARC path on EKE trends and variability, and its relation to changes in the wind stress curl, demonstrating how the ARC is shaped both by prominent bathymetric features along its path and a shifting wind regime.

2. Data and methods

In order to distinguish the ARC from the AC and Retroflection Region, the study is restricted to the box defined by 36.125°-46.125°S and 20.125°-70.325°E based on previous hydrological work done in this region by Lutjeharms and Ansorge (2001). Following Boebel and Barron (2003), the maximum gradient within the Sea Surface Height (SSH) fields is used as a proxy for the location of the ARC. Boebel and Barron (2003) showed that this proxy is aligned with the maximum currents of the ARC measured by floats and acoustic Doppler current profiler (ADCP).

The analysis was conducted on a gridded satellite altimeter product obtained from Copernicus. Absolute dynamic SSH topography (ADT) is calculated using data from all altimeter missions: Jason-3, Sentinel-3 A, HY-2 A, Saral/AltiKa, Cryosat −2, Jason-2, Jason-1, T/P, ENVISAT, GFO, ERS1/2 and is processed by the DUACS multimission altimeter data processing system. Its spatial resolution is 0.25° x 0.25° with a temporal resolution consisting of daily means spanning over 27 years (1993–2019).

The wind stress curl data is from the IFREMER CERSAT Global Blended Mean Wind Fields procured from Copernicus, which includes wind components (meridional and zonal), wind modulus, wind stress, wind stress curl and divergence. The 6-hourly blended wind product makes use of remotely sensed surface winds derived from all available scatterometers and radiometers. Its spatial resolution is 0.25° x 0.25° and provides data for the years 1994–2016.

The location of the ARC path (maximum velocity) was calculated by finding the point of maximum SSH gradient along each longitude line on the grid (201 longitude points by 40 points) within the chosen region, following the methodology of Boebel and Barron (2003). Together, these points of maximum SSH gradient provided a representation of the ARC path for each day (9861 days) (Fig. 1). In order to verify this method and confirm its efficiency in locating the ARC, the method was also applied to SST data (a gridded 0.25° x 0.25° product developed by CLS Production Unit and obtained through a combination between satellite and in-situ data, procured from Copernicus. It consists of 3D Temperature, Salinity, Heights, Geostrophic Currents and Mixed Layer Depth). A comparison between points of maximum gradient revealed an agreement at a vast majority of the locations examined.

While eddies do appear in this region and may have higher velocities than the current, the life span of a typical eddy at a specific location is a few weeks and thus they do not greatly affect the timeseries at the timescales addressed here. Temporal variability and long term trends in the equatorward–poleward migration of the ARC path were calculated at each longitude (201 longitude lines on the grid in the chosen region) along the length of the ARC in order to examine changes in the ARC path over the satellite era. Trends were calculated by fitting a straight line onto the ARC path latitude time series at each longitude grid between 20.125°-70.325°E.

The geostrophic currents (u and v) are derived from the ADT and represent the northward and eastward geostrophic sea water velocity. EKE is computed from the geostrophic current perturbations relative to the annual mean according to: EKE= $0.5(v'^2+u'^2)$ where $v' = v-\overline{v}$ and $u' = u-\overline{u}$, and $\overline{u}$ and $\overline{v}$ are the annual mean for each year.

EKE and wind stress curl decadal trends were calculated by using linear regression analysis on the EKE and wind stress curl data respectively. The EKE field was also averaged within the ARC study region (36.125°-46.125°S and 20.125°-70.325°E) to provide a single area mean EKE value for each of the time steps. The seasonal cycle of the EKE was examined by averaging the annual EKE levels of each season. Summer was defined as January–March and winter as June–August in accordance with the seasonality of the South Indian Ocean (Ffield et al., 1997; Behara and Yamagata, 2001). In addition to calculating the EKE with the annual mean, it was recalculated using a 6-month filter and compared to a 24-month filter, in order to assess the impacts of additional variability at seasonal time scales in our standard EKE. Although the amplitude of EKE is reduced with the 6-month filter, there is no significant difference between the trend of the 6-month filtered time-series and the 24-month filtered time-series and therefore our conclusion is not qualitatively affected if seasonal signal is removed from our standard EKE.

Certain characteristics of the current were present at all temporal resolutions, particularly the three meanders at the western section of the current (20°-37°E) and the slight shift to the south after 50°E. The bathymetry of the region was examined in order to investigate its influence on the nature of the path and to examine the extent of the relationship between the location of the quasi-stationary meanders along the current and the regional bathymetric features. The bathymetry data used was the 2014 GEBCO Gridded Bathymetry Data.

Calculations for f/H were utilized in order to examine the effects of bottom steering on the path of the ARC. The Coriolis component, f, was calculated for the entire grid as f = 2 Ωsin(Latitude) where Ω is 2π / 1 day in MKS units. It was then divided by H, height of the water column, based on the GEBCO bathymetry grid.

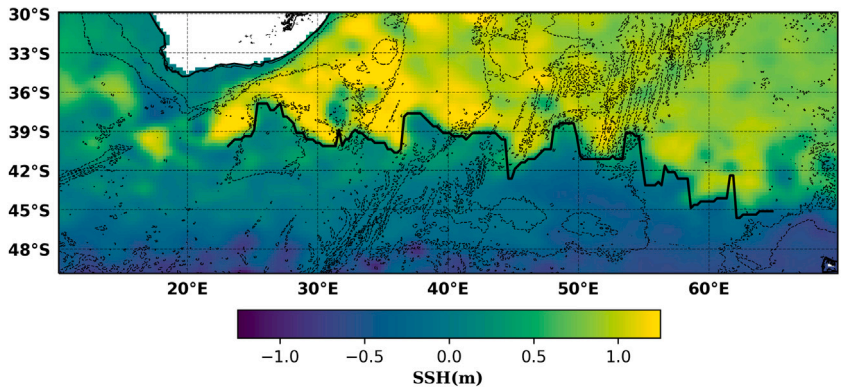

Fig. 1. Representation of the points of maximum SSH gradient for one time step (one day, 20th of July 1993) (thick black line) over the SSH contours for that same day (see colorbar). Regional bathymetry in thin black contours.

3. Results

3.1. ARC path analysis

3.1.1. Mean path

As with the findings of Yang et al. (2020), over the 27-year period examined here, the position of the ARC was relatively stable along its entire path, with the eastern portion of the current displaying a mean poleward migration of 0.015 degrees per year, in comparison to the larger shifts of other western boundary current extensions (Fig. 2a). The current has several quasi-stationary meanders (Fig. 2b) that stand out at nearly every temporal resolution explored (monthly mean, annual mean, 5-year mean and 27-year mean), most notably, a series of meanders at the western-most region of the current (20°-39°E). While there is considerable variability at monthly timescales due to the eddying nature of the current, over scales above the subseasonal, the path of the current is stable in relation to other WBC extentions (Lee and Cornillon, 1996). The terms used to refer to the meanders in previous studies (Boebel et al., 2003) and which will be utilized here for the sake of clarity are T1 (Trough 1-27°E), T2 (Trough 2-33°E) and T3 (Trough 3-39°E) for the meander troughs and C1 (Crest 1-30°E) and C2 (Crest 2-35°E) for the troughs between the crests (Fig. 2b). One previously undescribed feature that stands out is a southward swerve in the current path at 55°E which will be referred to as SWS (Southward Swerve).

3.1.2. Variability and trend

While the ARC meanders are quasi-stationary between 20°E and 40°E, there is a degree of variability in the latitude of the mean path throughout the current's entirety. The meridional variability of the ARC path varies between regions along the current, much like the other aspects of the current. The variability of the current position appears to be closely related to the presence of the quasi-stationary meanders described in Section 3.1 and by association, to the bathymetry of the region. The features T1, T2, T3, C1, C2 in the west and SWS in the east are characterized with a low degree of variability while areas linking these features tend to vary more in their meridional position (Fig. 2c), emphasizing the role of bathymetry in shaping the path of the ARC. The areas with the highest degree of variability are located adjacent to the bathymetric features, i.e. the Agulhas Plateau, Transkei Rise, the SWIR and the Kerguelen Islands.

The ARC path timeseries reveals a significant (95%, $p < 0.05$) trend in the migration of the current (Fig. 2a, also shown in blue and red in Fig. 2b) of up to 0.03° degrees latitude/year. However, the migration is not uniform in its direction. While the western region (20°E to 48°E) of the ARC appears to be migrating predominantly equatorward at a rate of 0.021 degrees latitude/year, the eastern region (48°E to 65°E)is migrating on average, poleward at a rate of 0.015 degrees latitude/year .

As with the ARC migrational trends, the regional wind stress curl (Fig. 3d) exhibits a complex pattern of positive and negative trends. While it is apparent that throughout most of the region there is an increase in wind stress curl, the trends along the path of the AC and ARC are relatively weak (across the SWIR), especially east of 45° where the trends are negative in several regions (50°E, 55°E, 60°E), coinciding with the strongest poleward trends in the path of the ARC.

3.2. EKE trends and variability

The EKE in the region follows a bi-modal distribution, demonstrating that the region follows a seasonal cycle of higher (lower) kinetic energy levels in the summer (winter) (Fig. 3a). In particular, the EKE timeseries reveals an increase in EKE between 1994 and 2011. The linear trend for the monthly-mean EKE is relatively small, 0.01 ± 0.050 (cm/s)/month (95%, p value = 0.83) and the slope is not significantly different from zero (not shown). However, the mean EKE values for the summer period (January–March) show a relatively rapid increase in EKE (Fig. 3b) with a significant (95%, p value = 0.044) linear trend of 3.42 ± 1.564 (cm/s)/year accumulating to an increase of approximately 10% between the aforementioned years. The mean EKE values for the winter (June–August) have no significant trend.

The EKE in the region exhibits a complex pattern of positive and negative trends all along the ARC (Fig. 3c). While the trend in the Agulhas Current, the Agulhas Retroflection region and C1 is mostly positive there are large areas of negative trends along the path of the ARC, the most notable of which are around C2 and over the SWIR.

The mean EKE levels along the ARC vary with a clear distinction between the western section (24°-40°E), the central section (40°-52°E) and the eastern section (52°-65°E) of the current (Fig. 4b). The western section is characterized with the highest levels of EKE with values of up to 2500 cm^2s^{-2}. The central section displays relatively low levels of EKE with values of 1000–1500 cm^2s^{-2}. EKE levels in the eastern region have similar peak values as in the western region but not as abundantly and concentrated mostly around SWS.

Similar to the characteristics of the ARC path, the EKE pattern corresponds with the bathymetry of the region (Fig. 4b). Areas with prominent bathymetric features are associated with low levels of EKE. This is most noticeable across the SWIR which has relatively low levels of EKE. The EKE values rise again after the eastern boundary of the ridge only to drop off just before the Kerguelen Islands, producing a shape that resembles the shape of the bathymetric features below the surface. Changes in wind surface forcing have a rapid barotropic response which modifies the bottom stress between ocean and bathymetry (Gille et al., 2004). With the increase in wind stress curl (Fig. 3d), the meanders adjust quickly to the change (Fig. 4a) by crossing f/h contours (Marshall and Stephens, 2001) defined by the Coriolis parameter f and the water depth h (Thompson and Naveira Garabato,

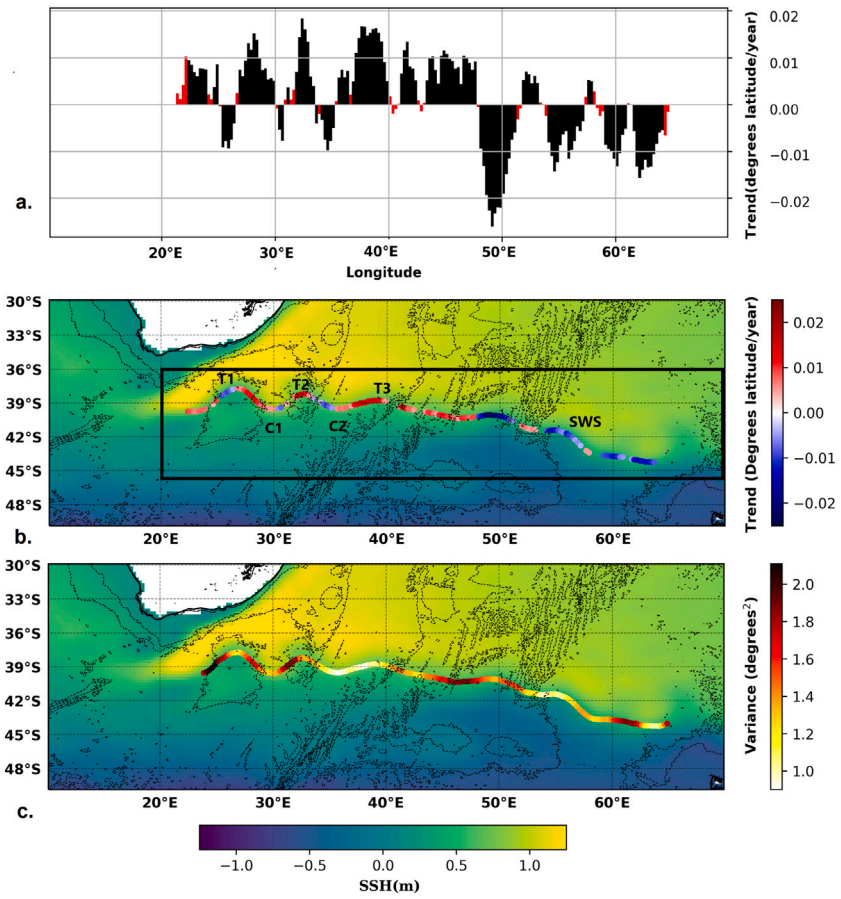

Fig. 2. a. The migration trend of the ARC (degrees latitude/year) at each longitude line in the study region. Black bars represent where the trend is significant. b. The mean path of the ARC averaged over 27 years (1993–2019) (representing points where there is a significant migration of the ARC path (degrees latitude/year) in blue (poleward) and red (equatorward) (see side colorbar)) overlain on the averaged SSH (see bottom colorbar) and regional bathymetry (black contours). Black rectangle represents limited study region. c. Variance (degrees^2) of the mean latitude of the ARC path over 27 years (1993–2019) (black/red/yellow, see side colorbar) overlain on the averaged SSH (see bottom colorbar) and regional bathymetry (black contours).

2014). The western region of the current exhibits an equatorward trend while the eastern region shift is predominantly poleward. This indicates that the western intensification and poleward shift of WBC's and their extensions that has been documented in the literature (Yang et al., 2016) is manifesting differently in each section. The western region, which interacts intensely with the bottom topography and has increased wind stress curl, shifts equatorward while the eastern section of the ARC (which is less topographically bound) migrates polewards due to a decrease in wind stress curl (Fig. 3d) and poleward migration of the westerly winds (Yang et al., 2016). An examination of the correlation (Pearson's r) between the mean wind stress curl time series and the average latitude of the ARC reveals a significant ($r = 0.423$, $p < 0.05$) correlation in the eastern (east of 47° E) section of the ARC with wind leading by 3 months. No significant correlation was found in the western section of the current.

4. Discussion

4.1. ARC path

Like other WBC extensions, the ARC responds to the gyre-wide transport driven by the curl of the wind stress exerted on the ocean surface (Backeberg et al., 2012). The regional bottom topography, however, also plays a key role in guiding the position of the current, leading to quasi-stationary meanders that are apparent in the time-mean path (Chao, 1994; Boebel et al., 2003; Bower and von Appen, 2008). Our results show that along the path of the ARC, there is less variability in the meridional position of the current at the troughs and crests of these quasi-stationary meanders than for the segments in between them (Fig. 2c).

The apparent stability in the location of the ARC meanders is in contrast to analogous WBC extensions such as the Gulf Stream Extension in which the meanders propagate downstream (Lee and Cornillon, 1996). Observations of the ARC mean path plotted over the map of the regional bathymetry (Fig. 2b, red and blue line) suggest a close relationship between the locations of the quasi-stationary features and the bathymetric features. Bottom steering has been shown to be important in WBC extension systems (Chao, 1994; Delman et al., 2015) through a potential vorticity mechanism (Cushman-Roisin and Beckers, 2010). As a result, the ARC forms the following features described in Boebel et al. (2003): a first standing meander (T1,C1 - 38°S, 27°E) is present around the Agulhas Plateau, followed by the second meander (T2,C2 - 38.5°S, 33°E) over the southern elongation of the Mozambique Plateau named the Transkei rise (Gohl et al., 2011). The third meander, T3 (39°S, 39°E), appears as the path of the current reaches the western most point of the Southwest Indian Ridge (SWIR), while SWS (42°S, 55°E) corresponds to the deepening at the eastern most point of the SWIR.

An examination of the ARC's mean path in the context of f/H contours (Fig. 4a), shows that in the entire eastern (east of 48°E) section of the ARC, it does not cross an f/H contour, and thus could be thought to be less constrained by bathymetry (Marshall and Stephens, 2001) when compared to the western part of the ARC, which interacts with more complex and steeper bathymetry. This phenomena can also be seen in a quasi-stationary meander in the path of the Kuroshio

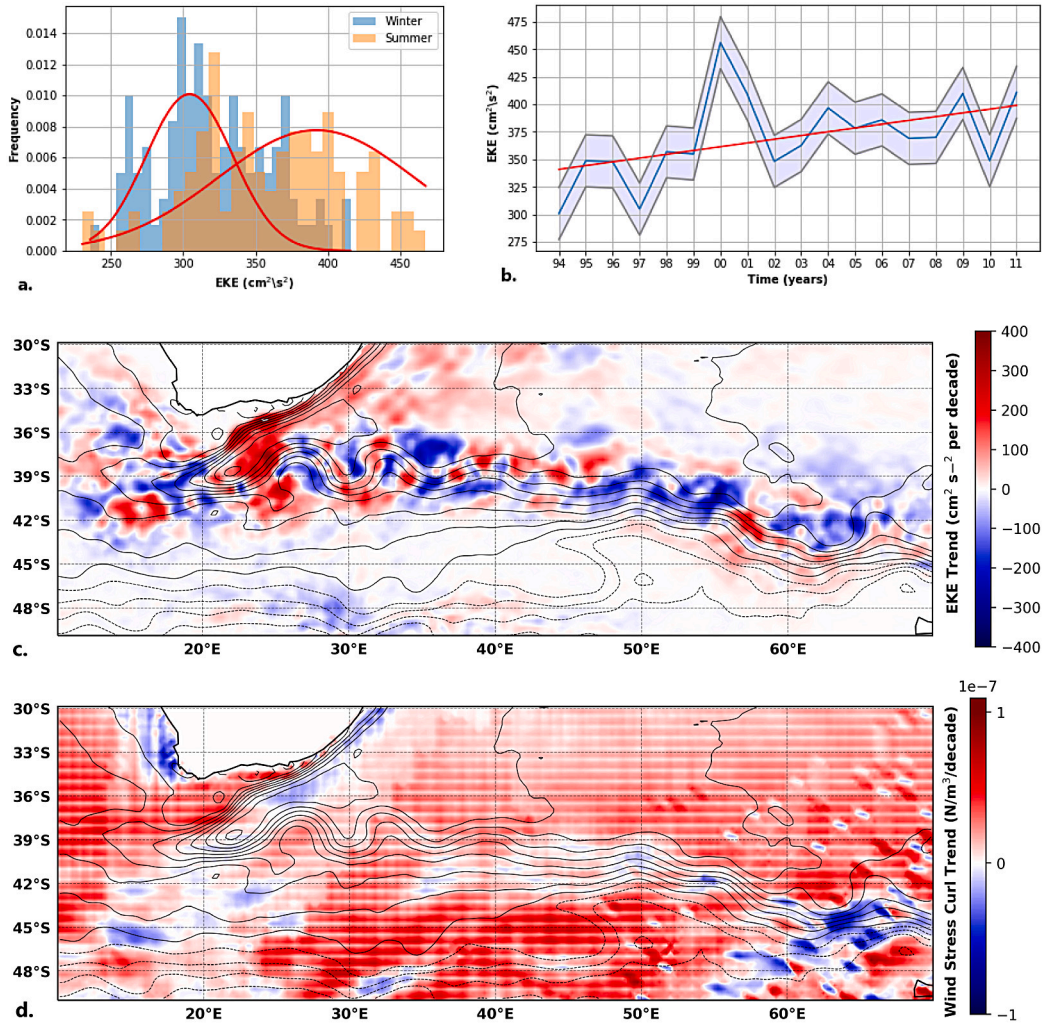

Fig. 3. a. Histogram of the seasonal distribution of mean EKE levels (cm^2 $s^{-}2$) in the ARC region, winter in blue and summer in orange with a density estimate in red. b.Mean summer (January–March) EKE levels (cm^2 $s^{-}2$) in the ARC region (20°-70°E) years 1994–2011 (r^2 = 0.48, $p < 0.05$). Standard deviation shaded, linear regression line in red. c.Decadal EKE trends (cm^2 $s^{-}2$ / decade) derived from altimetry for 1993–2019 (see side colorbar) with SSH (m) contours in black lines. d. Decadal wind stress curl trend (N/m^3 / decade) for 1994–2016 (see side colorbar) with SSH (m) contours in black lines.

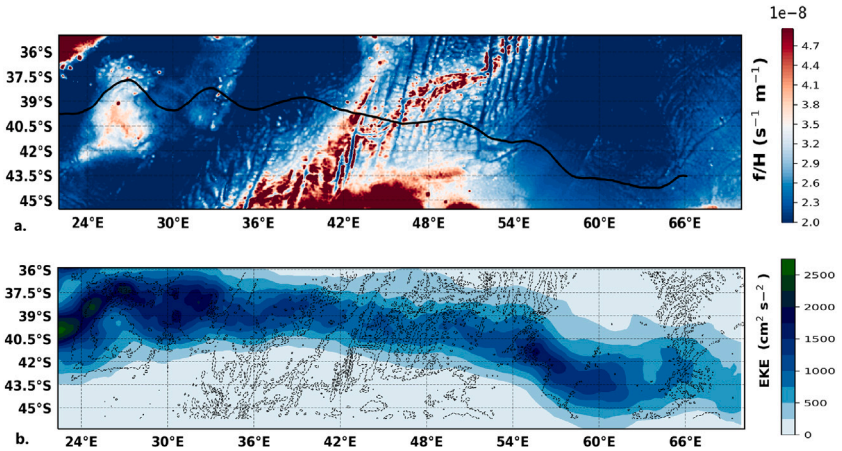

Fig. 4. a. Mean path of the ARC (black line) plotted over contours of f/H (see side colorbar). b. The mean EKE (cm^2s^{-2}) of the ARC averaged over 27 years (1993–2019). Overlaid in contours is the regional bathymetry (500 m intervals).

(33°N 140°E) (Delman et al., 2015; Chao, 1994). The ARC is deflected equatorward over ridges (lower h and f) and polewards over troughs.

4.2. Migration of the ARC

Analogous WBC extensions such as the Kuroshio Extension have been shown to migrate meridionally as a response to changes in either the main WBC (Kuroshio Current) or to other neighboring currents and fronts (in the case of the Kuroshio Extension it was the Sub-Arctic Frontal Zone) (Nakamura and Kazmin, 2003). Given the proximity of the Antarctic Circumpolar Current to the ARC and that it has been shown to be insensitive to long-term change (Böning et al., 2008; Gille, 2014), it is likely that it acts as a stabilizing agent for the ARC.

Yang et al. (2020) (using a different methodology to that used here) show that the part of the current eastward of 40°E is migrating poleward. While our findings confirm that the majority of the length of the current is migrating poleward, the eastern and western parts of the current actually show opposing trends, both of which are statistically significant. The shift from the equatorward trend in the west to the poleward trend in the east occurs at 48°E, and coincides with the western-most edge of shallower bathymetry of the SWIR. The migrational pattern seen along the ARC also resembles the pattern revealed in the wind stress curl field (Fig. 3d). Along the ARC, areas with increased (decreased) wind stress curl align with areas showing equatorward (poleward) migration (i.e 50°E, 55°E, 60°E). These patterns in the wind stress curl have been linked to SST variations along the ARC as a reaction to accelerations and decelerations of the westerly winds blowing across SST fronts (Chelton et al., 2004; O'Neill et al., 2005). It should be noted that the observed shift in the western part of the ARC is larger than the shift in the eastern part, highlighting the influence that the choice of domain has when looking at the mean migration of the ARC system or in fact the southern edge of the Indian Ocean subtropical gyre as a whole.

4.3. Increase in Eddy kinetic energy

Another form of intensification that has been highlighted in the ARC is an increase in EKE, particularly during the austral summer when the EKE values peak (Fig. 3b). This is in agreement with a recent study (Hogg et al., 2015) that shows strong increases in the EKE of the Pacific and Indian basins which was well correlated with regional wind stress with a 1–3 year lag. The bi-modal distribution shown in Fig. 3a indicates that EKE in the ARC follows a similar semi-annual seasonal cycle as does the South Indian ocean gyre. Work done on the seasonal circulation of the South Indian Ocean (Ffield et al., 1997) has shown a maximum transport in the ARC during February–March and a minimum transport during June–July, this is consistent with our findings regarding the months with the maximum/minimum EKE values. Reported transports of the ARC range from 55 Sv during winter to 70 Sv during summer, with a mean value of 65 Sv. These differences have been partially attributed (Ffield et al., 1997) to the meridional movement and strength of the South Indian Ocean Gyre. This strong decrease during June–July might explain why, although regional winds have been shown to be on the rise, the increase in EKE during the summer period is significant while no significant increase to EKE has been observed during the winter months.

As shown in Fig. 4b, the mean EKE field over the ARC can be divided into three regions. The reason that the EKE values in the western region (24°-40°E), the central region (40°-52°E) and the eastern region (52°-65°E) vary is most likely due to several factors. The most notable of these are the vicinity of the region to the Agulhas Current and the Agulhas Retroflection area, levels of bathymetric influence and the interaction with neighboring currents i.e the Antarctic Circumpolar Current. Local peaks in EKE levels are usually the result of baroclinic and barotropic instabilities generated by strong velocity gradients (Hakkinen and Rhines, 2009) such as those found in the AC and AR. Additional contributors to the EKE variability are Ekman pumping (Qiu and Chen, 2010), wind forcing and frontogenesis (which is most prominent in areas with strong SST gradients like the ARC). The combination of the western region's vicinity to the AC and AR regions together with the relatively shallow depths and prominent bathymetric features that may enhance turbulence, lead it to have the highest EKE levels of the three. While we witness a decrease in EKE throughout the central region (over the SWIR), there is a slight increase in EKE levels in the eastern region which indicates that the SWIR might be acting as an EKE dampener.

Examination of seasonal variations of the large-scale geostrophic flow field and EKE based on altimetric data (Scharffenberg and Stammer, 2010) revealed annual changes in all western boundary current systems due mainly to seasonally modulated strength changes in the Sverdrup circulation. In the midlatitudes, due to changes in the wind-driven barotropic circulation, the EKE field changes in its amplitude on the annual period, peaking in the summer. Our results indicating an increase in EKE (Fig. 3b), may also be related to the broadening of the Agulhas in response to wind intensification (Fig. 3d), shown by Beal and Elipot (2016) from mooring observations and rising oceanic temperatures in the Agulhas Region (Han and Yan, 2018). The implications of increased EKE are not fully understood (Zhu et al., 2018), but may include enhanced primary production Falkowski et al. (1991), elevated mixing (Naveira Garabato et al., 2011; Thompson and Sallée, 2012) and increased ocean–atmosphere interactions. Further exploration of these implications will be important for understanding the role of WBC and their extensions in the global carbon cycle. Understanding the role of vertical mixing in air–sea interaction is essential for improving model calculations of heat flux and carbon exchange. The ARC is the largest source of EKE in the Indian Ocean in addition to acting as a major CO_2 sink (Takahashi et al., 2009; Scharffenberg and Stammer, 2010). Improved observations of WBC extensions are essential, as is the need to improve how models resolve eddy activity in such regions with increasing EKE.

Declaration of competing interest

The authors declare that they have no known competing financial interests or personal relationships that could have appeared to influence the work reported in this paper.

Acknowledgments

Fadida, Y was funded by the South African Environmental Observation Network and their contribution toward this research is hereby acknowledged. Opinions expressed and conclusions arrived at are those of the authors and are not necessarily to be attributed to SAEON. The main product used in this study was the GLOBAL OCEAN GRIDDED L4 SEA SURFACE HEIGHTS AND DERIVED VARIABLES REPROCESSED (1993-ONGOING) reprocessed dataset which was obtained by merging the measurements from the different altimeter missions and was procured via Copernicus marine environment monitoring service, with details of its configuration and access to data available at http://marine.copernicus.eu. The SST product used for further analysis and method verification is the MULTI OBSERVATION GLOBAL OCEAN 3D TEMPERATURE SALINITY HEIGHT GEOSTROPHIC CURRENT AND MLD, procured via Copernicus marine environment monitoring service, with details of its configuration and access to data available at http://marine.copernicus.eu. The wind stress product procured through Copurnicus was the GLOBAL OCEAN WIND L4 REPROCESSED 6 HOURLY OBSERVATIONS , details of its configuration and access to data available at http://marine.copernicus.eu. Bathymetry data used was the 2014 GEBCO Gridded Bathymetry Data, with details of its configuration and access to data available at https://www.gebco.net

This is PMEL publication number 4989.

References

Backeberg, B.C., Penven, P., Rouault, M., 2012. Impact of intensified Indian ocean winds on mesoscale variability in the agulhas system. Nature Clim. Change 2 (8), 608–612. http://dx.doi.org/10.1038/nclimate1587.

Beal, L.M., Elipot, S., 2016. Broadening not strengthening of the agulhas current since the early 1990s. Nature 540 (7634), 570–573. http://dx.doi.org/10.1038/nature19853.

Behara, S., Yamagata, T., 2001. Subtropical SST dipole events in the southern Indian ocean. Geophys. Res. Lett. (2), 1–3. http://dx.doi.org/10.1029/2000GL011451.

Biastoch, A., Böning, C.W., Schwarzkopf, F.U., Lutjeharms, J.R.E., 2009. Increase in agulhas leakage due to poleward shift of southern hemisphere westerlies. Nature 462 (7272), 495–498. http://dx.doi.org/10.1038/nature08519, http://www.ncbi.nlm.nih.gov/pubmed/19940923, http://www.nature.com/articles/nature08519.

Boebel, O., Barron, C., 2003. A comparison of in-situ float velocities with altimeter derived geostrophic velocities. Deep Sea Res. Part II 50 (1), 119–139. http://dx.doi.org/10.1016/S0967-0645(02)00381-8, https://www.sciencedirect.com/science/article/pii/S0967064502003818.

Boebel, O., Rossby, T., Lutjeharms, J., Zenk, W., Barron, C., 2003. Path and variability of the Agulhas Return Current. Deep-Sea Res. Part II 50 (1), 35–56. http://dx.doi.org/10.1016/S0967-0645(02)00377-6.

Böning, C.W., Dispert, A., Visbeck, M., Rintoul, S.R., Schwarzkopf, F.U., 2008. The response of the antarctic circumpolar current to recent climate change. Nat. Geosci. 1 (12), 864–869. http://dx.doi.org/10.1038/ngeo362.

Bower, A.S., von Appen, W.J., 2008. Interannual variability in the pathways of the North Atlantic Current over the mid-atlantic ridge and the impact of topography. J. Phys. Oceanogr. 38 (1), 104–120. http://dx.doi.org/10.1175/2007JPO3686.1.

Cetina-Heredia, P., Roughan, M., van Sebille, E., Coleman, M.A., 2014. J. Geophys. Res. (119), 3868–3882. http://dx.doi.org/10.1002/2014JC010089.Received, http://onlinelibrary.wiley.com/doi/10.1002/jgrc.20353/abstract.

Chang, Y.C., Tseng, R.S., Chen, G.Y., Chu, P.C., Shen, Y.T., 2013. Ship routing utilizing strong ocean currents. J. Navig. 66 (6), 825–835. http://dx.doi.org/10.1017/S0373463313000441.

Chao, S.-Y., 1994. Zonal jets over topography on a beta-plane, with applications to the kuroshio extension over the shatsky rise. J. Phys. Oceanogr. 24 (7), 1512–1531. http://dx.doi.org/10.1175/1520-0485(1994)024<1512:zjotoa>2.0.co;2.

Chelton, D.B., Schlax, M.G., Freilich, M.H., Milliff, R.F., 2004. Satellite measurements reveal persistent small-scale features in ocean winds. Technical Report, www.sciencemag.org.

Combes, V., Matano, R.P., 2014. Trends in the Brazil/malvinas confluence region. Geophys. Res. Lett. 41 (24), 8971–8977. http://dx.doi.org/10.1002/2014GL062523.

Cushman-Roisin, B., Beckers, J.-M., 2010. Introduction to geophysical fluid dynamics. Physical and numerical aspects. Analysis 101, 786, http://books.google.com/books?hl=en&lr=&id=4g-6iX6EQ8YC&oi=fnd&pg=PP2&dq=Introduction+to+Geophysical+Fluid+Dynamics+Physical+and+Numerical+Aspects&ots=xLX8fNZYYL&sig=oatMPBCOzDtnUt9wORBhBJZ5BM0.

Delman, A.S., McClean, J.L., Sprintall, J., Talley, L.D., Yulaeva, E., Jayne, S.R., 2015. Effects of eddy vorticity forcing on the mean state of the kuroshio extension. J. Phys. Oceanogr. 45 (5), 1356–1375. http://dx.doi.org/10.1175/JPO-D-13-0259.1, http://journals.ametsoc.org/doi/10.1175/JPO-D-13-0259.1.

Deser, C., Alexander, M.A., Timlin, M.S., Deser, C., Alexander, M.A., Timlin, M.S., 1999. Evidence for a wind-driven intensification of the kuroshio current extension from the 1970s to the 1980s. J. Clim. 12 (6), 1697–1706. http://dx.doi.org/10.1175/1520-0442(1999)012<1697:EFAWDI>2.0.CO;2, http://journals.ametsoc.org/doi/abs/10.1175/1520-0442%281999%29012%3C1697%3AEFAWDI%3E2.0.CO%3B2.

Dinezio, P.N., Clement, A.C., Vecchi, G.A., Soden, B.J., Kirtman, B.P., Lee, S.-K., 2009. Climate response of the equatorial Pacific to global warming. J. Clim. - Am. Meteorol. Soc. http://dx.doi.org/10.1175/2009JCLI2982.1, https://journals.ametsoc.org/doi/pdf/10.1175/2009JCLI2982.1.

Dong, S., Kelly, K.A., 2003. Heat budget in the gulf stream region: The importance of heat storage and advection. Technical Report, University of Washington, http://shoni2.princeton.edu/ftp/lyo/journals/Dong_Kelly_heat_budget_GS_JPO2003.pdf.

Falkowski, P.G., Ziemann, D., Kolber, Z., Bienfang, P.K., 1991. Role of eddy pumping in enhancing primary production in the ocean. Nature 352 (6330), 55–58. http://dx.doi.org/10.1038/352055a0, http://www.nature.com/doifinder/10.1038/352055a0.

Ffield, A., Toole, J., Wilson, D., 1997. Seasonal circulation in the south Indian ocean. Geophys. Res. Lett. 24 (22), 2773–2776.

Friehe, C.A., Shaw, W.J., Rogers, D.P., Davidson, K.L., Large, W.G., Stage, S.A., Crescenti, G.H., Khalsa, J.S., Greenhut, G.K., Li, F., 1991. Air-sea fluxes and surface layer turbulence around a sea surface temperature front. J. Geophys. Res. 96 (C5), 8593–8609. http://dx.doi.org/10.1029/90JC02062, http://onlinelibrary.wiley.com/doi/10.1029/90JC02062/full.

Gille, S.T., 2014. Meridional displacement of the antarctic circumpolar current. Phil. Trans. R. Soc. A 372 (2019), http://dx.doi.org/10.1098/rsta.2013.0273.

Gille, S., Metzger, E.J., Tokmakjan, R., 2004. Seafloor topography and ocean circulation. Technical Report, https://apps.dtic.mil/sti/citations/ADA423293.

Gohl, K., Uenzelmann-Neben, G., Grobys, N., 2011. Growth and dispersal of a Southeast African large igneous province. South Afr. J. Geol. 114 (3–4), 379–386. http://dx.doi.org/10.2113/gssajg.114.3-4.379.

Goni, G.J., Bringas, F., DiNezio, P.N., 2011. Observed low frequency variability of the Brazil current front. J. Geophys. Res. 116 (C10), C10037. http://dx.doi.org/10.1029/2011JC007198.

Gordon, A.L., 1986. Interocean exchange of thermocline water. J. Geophys. Res. 91 (C4), 5037. http://dx.doi.org/10.1029/jc091ic04p05037.

Gray, A.R., Palter, J.B., 2017. the Role of Western Boundary Current Regions in the Global Carbon Cycle. Vol. 15, pp. 1–4. http://dx.doi.org/10.5065/D6SJ1JB2.

Hakkinen, S., Rhines, P.B., 2009. Shifting surface currents in the northern north atlantic ocean. J. Geophys. Res. 114 (C4), C04005. http://dx.doi.org/10.1029/2008JC004883, http://doi.wiley.com/10.1029/2008JC004883.

Han, L., Yan, X.-H., 2018. Warming in the agulhas region during the global surface warming acceleration and slowdown. Sci. Rep. 8 (1), 13452. http://dx.doi.org/10.1038/s41598-018-31755-1, http://www.nature.com/articles/s41598-018-31755-1.

Hogg, A.M., Meredith, M.P., Chambers, D.P., Abrahamsen, E.P., Hughes, C.W., Morrison, A.K., 2015. Recent trends in the southern ocean eddy field. J. Geophys. Res. 120 (1), 257–267. http://dx.doi.org/10.1002/2014JC010470, http://doi.wiley.com/10.1002/2014JC010470.

Kwon, Y.O., Deser, C., 2007. North Pacific decadal variability in the community climate system model version 2. J. Clim. 20 (11), 2416–2433. http://dx.doi.org/10.1175/JCLI4103.1.

Lee, T., Cornillon, P., 1996. Propagation of gulf stream meanders between 74 and 70 w. J. Phys. Oceanogr. 26 (2), 205–224. http://dx.doi.org/10.1175/1520-0485(1996)026<0205:POGSMB>2.0.CO;2.

Liu, W.T., Xie, X., Niiler, P.P., 2007. Ocean-atmosphere interaction over agulhas extension meanders. J. Clim. 20 (23), 5784–5797. http://dx.doi.org/10.1175/2007JCLI1732.1.

Lutjeharms, J.R., Ansorge, I.J., 2001. The agulhas return current. J. Mar. Syst. 30 (1–2), 115–138. http://dx.doi.org/10.1016/S0924-7963(01)00041-0.

Marshall, D.P., Stephens, J.C., 2001. On the insensitivity of the wind-driven circulation to bottom topography. J. Mar. Res. 59 (1), 1–27. http://dx.doi.org/10.1357/002224001321237344.

Nakamura, H., Kazmin, A., 2003. Decadal changes in the north Pacific oceanic frontal zones as revealed in ship and satellite observations. J. Geophys. Res. 108 (C3), 3078. http://dx.doi.org/10.1029/1999JC000085, http://doi.wiley.com/10.1029/1999JC000085.

Naveira Garabato, A.C., Ferrari, R., Polzin, K.L., 2011. Eddy stirring in the southern ocean. J. Geophys. Res. 116 (C9), C09019. http://dx.doi.org/10.1029/2010JC006818, http://doi.wiley.com/10.1029/2010JC006818.

Oey, L.-Y., Wang, J., Lee, M.-A., 2018. Fish catch is related to the fluctuations of a western boundary current. J. Phys. Oceanogr. 48 (3), 705–721. http://dx.doi.org/10.1175/JPO-D-17-0041.1, http://journals.ametsoc.org/doi/10.1175/JPO-D-17-0041.1.

Ohishi, S., Tozuka, T., Komori, N., 2016. Frontolysis by surface heat flux in the agulhas return current region with a focus on mixed layer processes: observation and a high-resolution CGCM. Clim. Dynam. 47 (12), 3993–4007. http://dx.doi.org/10.1007/s00382-016-3056-0.

O'Neill, L.W., Chelton, D.B., Esbensen, S.K., Wentz, F.J., 2005. High-resolution satellite measurements of the atmospheric boundary layer response to SST variations along the agulhas return current. J. Clim. 18 (14), 2706–2723. http://dx.doi.org/10.1175/JCLI3415.1.

Qiu, B., Chen, S., 2010. Eddy-mean flow interaction in the decadally modulating Kuroshio Extension system. Deep-Sea Res. Part II 57 (13–14), 1098–1110. http://dx.doi.org/10.1016/j.dsr2.2008.11.036, http://dx.doi.org/10.1016/j.dsr2.2008.11.036.

Richardson, P.L., 2007. Agulhas leakage into the Atlantic estimated with subsurface floats and surface drifters. Deep-Sea Res. Part I 54 (8), 1361–1389. http://dx.doi.org/10.1016/j.dsr.2007.04.010.

Ridgway, K.R., 2007. Long-term trend and decadal variability of the southward penetration of the east Australian current. Geophys. Res. Lett. 34, http://dx.doi.org/10.1029/2007GL030393, https://agupubs.onlinelibrary.wiley.com/doi/pdf/10.1029/2007GL030393.

Ridgway, K.R., Coleman, R.C., Bailey, R.J., Sutton, P., 2008. Decadal variability of East Australian current transport inferred from repeated high-density XBT transects, a CTD survey and satellite altimetry. J. Geophys. Res. 113 (C8), C08039. http://dx.doi.org/10.1029/2007JC004664, http://doi.wiley.com/10.1029/2007JC004664.

Sakamoto, T.T., Hasumi, H., Ishii, M., Emori, S., Suzuki, T., Nishimura, T., Sumi, A., 2005. Responses of the Kuroshio and the Kuroshio Extension to global warming in a high-resolution climate model. Geophys. Res. Lett. 32 (14), n/a–n/a. http://dx.doi.org/10.1029/2005GL023384, http://doi.wiley.com/10.1029/2005GL023384.

Scharffenberg, M.G., Stammer, D., 2010. Seasonal variations of the large-scale geostrophic flow field and eddy kinetic energy inferred from the TOPEX/Poseidon and Jason-1 tandem mission data. J. Geophys. Res. 115 (2), 1–29. http://dx.doi.org/10.1029/2008JC005242.

Small, R.J., DeSzoeke, S.P., Xie, S.P., O'Neill, L., Seo, H., Song, Q., Cornillon, P., Spall, M., Minobe, S., 2008. Air-sea interaction over ocean fronts and eddies. Dyn. Atmos. Oceans 45 (3–4), 274–319. http://dx.doi.org/10.1016/j.dynatmoce.2008.01.001.

Speich, S., Blanke, B., Madec, G., 2001. Warm and cold water routes of an O.G.C.M. thermohaline conveyor belt. Geophys. Res. Lett. 28 (2), 311–314. http://dx.doi.org/10.1029/2000GL011748, http://doi.wiley.com/10.1029/2000GL011748.

Takahashi, T., Sutherland, S.C., Wanninkhof, R., Sweeney, C., Feely, R.A., Chipman, D.W., Hales, B., Friederich, G., Chavez, F., Sabine, C., Watson, A., Bakker, D.C., Schuster, U., Metzl, N., Yoshikawa-Inoue, H., Ishii, M., Midorikawa, T., Nojiri, Y., Körtzinger, A., Steinhoff, T., Hoppema, M., Olafsson, J., Arnarson, T.S., Tilbrook, B., Johannessen, T., Olsen, A., Bellerby, R., Wong, C.S., Delille, B., Bates, N.R., de Baar, H.J., 2009. Climatological mean and decadal change in surface ocean pco2, and net sea-air CO2 flux over the global oceans. Deep-Sea Res. Part II 56 (8–10), 554–577. http://dx.doi.org/10.1016/j.dsr2.2008.12.009.

Thompson, A.F., Naveira Garabato, A.C., 2014. Equilibration of the antarctic circumpolar current by standing meanders. J. Phys. Oceanogr. 44 (7), 1811–1828. http://dx.doi.org/10.1175/JPO-D-13-0163.1, http://journals.ametsoc.org/doi/10.1175/JPO-D-13-0163.1.

Thompson, A.F., Sallée, J.-B., 2012. Jets and topography: Jet transitions and the impact on transport in the antarctic circumpolar current. J. Phys. Oceanogr. 42 (6), 956–972. http://dx.doi.org/10.1175/JPO-D-11-0135.1, http://journals.ametsoc.org/doi/10.1175/JPO-D-11-0135.1.

Tozuka, T., Cronin, M.F., 2014. Role of mixed layer depth in surface frontogenesis: The agulhas return current front. Geophys. Res. Lett. 41 (7), 2447–2453. http://dx.doi.org/10.1002/2014GL059624.

van Sebille, E., van Leeuwen, P.J., Biastoch, A., de Ruijter, W.P.M., 2010. On the fast decay of agulhas rings. J. Geophys. Res. 115 (C3), C03010. http://dx.doi.org/10.1029/2009JC005585, http://doi.wiley.com/10.1029/2009JC005585.

Wu, L., Cai, W., Zhang, L., Nakamura, H., Timmermann, A., Joyce, T., McPhaden, M.J., Alexander, M., Qiu, B., Visbeck, M., Chang, P., Giese, B., 2012. Enhanced warming over the global subtropical western boundary currents. Nature Clim. Change 2 (3), 161–166. http://dx.doi.org/10.1038/nclimate1353.

Yang, H., Lohmann, G., Krebs-Kanzow, U., Ionita, M., Shi, X., Sidorenko, D., Gong, X., Chen, X., Gowan, E.J., 2020. Poleward shift of the major ocean gyres detected in a warming climate. Geophys. Res. Lett. 47 (5), http://dx.doi.org/10.1029/2019GL085868, https://onlinelibrary.wiley.com/doi/abs/10.1029/2019GL085868.

Yang, H., Lohmann, G., Wei, W., Dima, M., Ionita, M., Liu, J., 2016. Intensification and poleward shift of subtropical western boundary currents in a warming climate. J. Geophys. Res. Oceans 1–15. http://dx.doi.org/10.1002/2016JC012335.Received, http://arxiv.org/abs/arXiv:1402.6991v1.

Zhu, Y., Qiu, B., Lin, X., Wang, F., 2018. Interannual eddy kinetic energy modulations in the agulhas return current. J. Geophys. Res. 123 (9), 6449–6462. http://dx.doi.org/10.1029/2018JC014333, http://doi.wiley.com/10.1029/2018JC014333.